

## **Integrated analysis of magnetic, gravity and multichannel seismic reflection data along a transect southeast of Sri Lanka, Bay of Bengal: New constraints**

**Maria Ana Desa<sup>1</sup>, M. V. Ramana<sup>2</sup>**

<sup>1</sup>Geological Oceanography, CSIR-National Institute of Oceanography, Goa 403 004 India

<sup>2</sup>Sagarika Apts, Street No. 1, Nagali Hills, Dona Paula, Goa 403 004 India

### **Abstract:**

Integrated analysis of high quality magnetic, gravity, bathymetry and multichannel seismic reflection data along a 1300 km long transect SK101 between the DSDP218/IODP1455 and ODP718 sites reveals the structure and evolutionary history of the underlying sedimentary load and basement. The smooth southward deepening bathymetry is pierced by several topographic highs of varying dimensions. Gravity does not mimic the bathymetry in general, and is as low as -75 mgal over a deep basement region. Magnetic anomalies depict significant variation along the transect, with chron A34 identified at its either end.

Multichannel seismic reflection data reveal sediment thickness up to 3 sec two-way travel time (TWT), but minimal (<0.1 sec TWT) over protruding basement highs. Intense folding/faulting of sediment and basement producing low amplitude, long wavelength topographic highs is observed towards south along the transect. Flower structures seen within the sedimentary load suggest intermittent strike-slip faulting. The basement highs lying at the southern end of NW-SE trending fracture zones may have formed as the spreading center rotated clockwise during the Middle Cretaceous period. An arcuate gravity low is due to the presence of a deep and old basement, overlain by thick sediments. A prominent step in the basement coinciding with an abrupt change in magnetic anomaly pattern probably indicates the concurrent presence of oceanic crust of different ages, as a consequence of the Middle Cretaceous major plate reorganisation.

## 1. Introduction

The Bay of Bengal lying between the East Coast of India and the Sunda Trench (Fig. 1), was formed due to the breakup of Eastern Gondwanaland, and subsequent seafloor spreading between India and Antarctica in the Early Cretaceous (Powell et al., 1988; Royer and Coffin, 1992; Ramana et al., 1994; Gibbons et al., 2013; Talwani et al., 2016). The Bay of Bengal is divided into two basins - the western and eastern basins, by the subsurface 85°E Ridge (Fig. 2a). This ridge is interpreted based on seismic records (Gopala Rao et al., 1997; Bastia et al., 2010; Desa et al., 2013) and its typical negative gravity anomaly signature (Liu et al., 1982).

Several plate reconstruction models have been generated to explain the evolution of the oceanic crust between India and Antarctica, since the Early Cretaceous (Powell et al., 1988; Royer and Coffin, 1992; Ramana et al., 2001; Gaina et al., 2007; Gibbons et al., 2013; Talwani et al., 2016). Recent models reveal that the oceanic crust underlying the Bay of Bengal (Fig. 2a) has formed due to two spreading episodes between India and Antarctica. The first occurred in the Early Cretaceous period in the NW-SE direction (Ramana et al., 1994; Talwani et al., 2016), and the crust thus generated is found in the western basin of the Bay of Bengal, around Sri Lanka and in the western Enderby Basin, East Antarctica (Fig. 1).

The second spreading episode between India and Antarctica occurred during the Middle Cretaceous period (Powell et al., 1988; Royer and Coffin, 1992; Desa and Ramana, 2016). This Middle Cretaceous period is known for its global-scale major plate reorganization (Matthews et al., 2012). This reorganization is associated with plume-related changes in spreading direction and rate, transfer of oceanic crust, and formation of plateaus, microcontinents, etc. (Kent et al., 2002; Nogi et al., 2004; Bernard et al., 2005; Desa et al., 2006). Since this period was also characterized by the geomagnetic long normal polarity epoch (Tarduno et al., 2001), tracing the detailed evolution of the oceanic crust using the standard magnetic method is rather difficult.

A change in spreading parameters occurred due to the arrival of the Kerguelen plume beneath Eastern India around 120 Ma (Kent, 1991), causing a part of the spreading ridge to jump northwards to the Rajmahal-Sylhet traps (Talwani et al., 2016). This ridge jump resulted in the formation and transfer of several microcontinents such as Elan Bank and Southern Kerguelen Plateau (Fig. 1), from the Indian plate to Antarctica plate (Kent et al., 2002; Gaina et al., 2007). Thereafter, seafloor spreading occurred in the eastern basin of the Bay of Bengal (Desa and Ramana, 2016), south of Sri Lanka (Fig. 2a), and their conjugate regions in the Enderby Basin during the Middle Cretaceous period (Desa et al., 2006;

Gibbons et al., 2013). The seafloor spreading direction also changed during this period, to become N-S by the Late Cretaceous period (Powell et al., 1988; Royer and Coffin, 1992; Bernard et al., 2005).

The Bay of Bengal is floored by the world's largest submarine fan, the Bengal Fan (Curry et al., 1982). The enormous sediment input derived due to erosion of the Himalayas has resulted in as much as 22 km thick sediments at the apex of the Bengal Fan (Curry, 1994). A network of turbidity channels distributes this sediment load up to south of the equator (Curry et al., 2003). Furthermore, the sediment distribution pattern has been interrupted by the N-S trending 85°E and Ninetyeast Ridges (Curry, 1994).

The 85°E Ridge lies buried beneath the Bengal Fan sediments in the northern Bay of Bengal (Curry et al., 1982; Liu et al., 1982). Based on its typical gravity anomaly signature, the ridge has been inferred to take an arcuate bend, south of 6°N, around Sri Lanka (Fig. 2a) to terminate at the Afanasy Nikitin seamount chain (ANS) (Curry and Munasinghe, 1991; Muller et al., 1993). The ANS is a prominent feature having a relief of more than 2 km, lying along 83°E, between 2° and 6°S (Fig. 2a). Earlier investigations have revealed that the ANS originated in the vicinity of a spreading ridge axis due to anomalous volcanism (eg. Goslin and Schlich, 1982). In contrast to the hypothesis of the arcuate bend of the 85°E Ridge, the ridge is inferred to continue southward as the 86°E Fracture Zone (FZ) (Kent et al., 1992; Desa and Ramana, 2016; Altenbernd et al., 2020). Furthermore, several contrasting hypotheses have been postulated for the origin of the 85°E Ridge, which are described in detail later.

The Ninetyeast Ridge extending from 35°S to about 17°N along the 90°E meridian, (Heezen and Tharp, 1964) is one of the longest linear topographic features in the world (Figs. 1 & 2a). DSDP and ODP results indicate that the ridge is an extrusive volcanic feature that formed subaerially or in shallow environment, and subsided with time (Von der Borch et al., 1974; Klootwijk et al., 1992). Paleomagnetic studies confirm that the ridge was attached to the Indian plate, and both have moved rapidly northward since Late Cretaceous (Pierce, 1978).

Several geophysical studies have been undertaken and valuable inferences have been drawn about the evolution of the Bay of Bengal. But we find that most of these studies have been carried out in the northern Bay of Bengal. A detailed geophysical investigation tracing the sedimentary and crustal evolution of the region south of Sri Lanka, was lacking. To fill this vital gap, geophysical data were acquired along a transect between the DSDP218 and ODP718 drill sites. In the present study, we conducted seismic stratigraphy, investigated the deformation signatures and traced the evolution of the basement along this transect. We present the significant findings of the integrated geophysical analysis in this paper.

## 2. The study area

The study area lies in the southern Bay of Bengal between the Comorin Ridge to the west and the Ninetyeast Ridge to the east (Fig. 2a). The NW-SE trending fracture zones off the southeastern coast of India and around Sri Lanka (Wessel et al., 2015) assert that the oceanic crust around Sri Lanka is the continuation of the western basin of the Bay of Bengal, and has evolved since the Early Cretaceous (Desa et al., 2006; Gibbons et al., 2013; Talwani et al., 2016).

The Middle Cretaceous crust lying between the youngest Early Cretaceous isochron M0 (120 Ma) and the oldest Late Cretaceous isochron A34 (83 Ma) (Gee and Kent, 2007) has been inferred in the eastern basin of the Bay of Bengal (Desa and Ramana, 2016). It extends from the apex of the Bay of Bengal at 20°N to about 8°N (Fig. 2a). The presence of Middle Cretaceous crust has also been proposed south of Sri Lanka (Ramana et al., 1997a). The disposition of the M0 and A34 isochrons south of Sri Lanka implies the presence of narrow and uneven extent of the Middle Cretaceous crust (Desa et al., 2006; 2009), as compared to that in the eastern basin of the Bay of Bengal.

The Late Cretaceous crust further south, is characterised by several N-S trending fracture zones (Powell et al., 1988; Royer and Coffin, 1992). The 86°E FZ is a large offset fracture zone in the Bay of Bengal with the older fracture zones truncating against it (Sclater and Fisher, 1974) (Fig. 2a). It offsets the Late Cretaceous crust south of Sri Lanka, left laterally by about 900 km. Its conjugate Kerguelen FZ in the Enderby Basin, off East Antarctica (Fig. 1) also depicts a large offset and is associated with prominent bathymetric and gravity signatures (Rotstein et al., 2001).

### 2.1 The 85°E Ridge

The ~N-S trending 85°E Ridge, in contrast to other aseismic ridges, is characterised by a prominent negative gravity anomaly (Curry et al., 1982; Liu et al., 1982). This feature has remained enigmatic till date with several contrasting hypotheses proposed for its origin. Curry and Munasinghe (1991) deduced that the ridge along with the Rajmahal Traps and ANS, is a trace of the Crozet hotspot. Kent et al. (1992) refuted this claim and proposed that the ridge is a northward continuation of the 86°E FZ. Another opinion was that the ridge and ANS might have been formed by a hotspot now located beneath the eastern Conrad Rise on the Antarctica plate (Muller et al., 1993). The 85°E Ridge may have formed due to volcanic emplacement during a short span of time when the Middle Cretaceous major plate reorganization took place (Ramana et al., 1997b). Krishna (2003) proposed that the 85°E Ridge, the buried hills and the ANS were formed by an unknown hotspot between 85 and 60 Ma. Anand et al. (2009) postulated that the ridge is a geomorphological feature within the sediments above the basement, north of 15°N latitude.

Recently, Desa et al. (2013) opined that the northern portion of the 85°E Ridge was emplaced in the Middle Cretaceous period as a pseudofault over which volcanism occurred subsequently. The northern portion of the 85°E Ridge is considered as a transform fault along which the spreading ridge jumped north around M0 time, under the influence of the Kerguelen plume (Talwani et al., 2016). The 85°E Ridge south of 12°N, is proposed to be the northward continuation of the 86°E FZ (Desa and Ramana, 2016). Based on recent OBS results, Altenbernd et al. (2020) found no indications for the bending of the 85°E Ridge towards the ANS, and postulated that the ridge is the northward continuation of the 86°E FZ.

## *2.2 Tectonic deformation*

The oceanic lithosphere of the Central Indian Ocean Basin (CIOB) hosts a diffuse plate boundary between the Indian, Capricorn and Australian plates (Wiens et al. 1985; Gordon et al., 1998). The occurrence of intense tectonic deformation was reported in this region (Fig. 1) based on high seismicity, unusual heat flow, gravity/geoidal anomalies and seismic records (Weissel et al., 1980; Geller et al., 1983). The compressional stress due to the collision of India with Eurasia, resulted in east-west striking folds and thrust faults causing significant crustal shortening (Wiens et al., 1985; Chamot-Rooke et al., 1993). Furthermore, the stress is relieved by earthquakes around topographic high regions, and as vertical movements over uniform lithosphere (Levchenko, 1992). East of the Ninetyeast Ridge, in the northwestern Wharton Basin, deformation is seen mostly as left lateral strike slip motion (Deplus et al., 1998; Stevens et al., 2020).

In the CIOB, the oceanic crust is deformed in two scales, (i) long-wavelength (100-300 km) anticlinal basement rises trending 70°E and terminating at fracture zones, and (ii) high-angle reverse faults of 5-20 km wide blocks superimposed on the anticlines having a mean length of 10 km and trend of 100°E (Neprochnov et al., 1988; Levchenko, 1992; Murthy et al., 1993). The high-angle reverse faults are caused due to reactivation of the pre-existing spreading center related fault fabric (Bull and Scrutton, 1990a) while selective abandonment of faults took place due to strain weakening (Delescluse et al., 2008).

Seismic stratigraphy and deep-sea drilling at ODP Leg 116 sites indicate that deformation began around ~8 Ma due to north-south compression of the Indian plate (Curry and Munasinghe, 1989; Cochran et al., 1990). Gordon et al. (1998) suggested that deformation may have begun as early as 18 Ma, while Krishna et al. (1998) opined that the deformation is periodic with cyclicity of about 3.5 m.y. Furthermore, the spatial extents of the discretely occurring deformation events (8 Ma, 4 Ma and 0.8 Ma) were mapped in the CIOB (Krishna et al., 2001).

### *2.3 Drilling and seismic information*

DSDP Leg 22 and ODP Leg 116 were conducted to infer the sedimentation history of the Bengal Fan in the northeastern Indian Ocean. The drilling results indicate that the recovered sediments are mostly terrigenous in origin brought in by the Ganga-Brahmaputra rivers. The upper Miocene unconformity marks the onset of deformation and divides the sediments into the pre-deformation and syn-deformation units. The Eocene unconformity, a hiatus increasing in duration down the fan between Paleocene and middle Eocene time, is postulated to indicate the timing of fan initiation after the initial India–Eurasia collision (Curry and Munasinghe, 1989).

Site 218 of DSDP Leg 22 drilled in the central Bengal Fan region penetrated 772 m to reach the Middle Miocene deposits (Von der Borch et al., 1974). Five lithologic units and four turbidity pulses were reported from Recent to Middle Miocene time. The seismic profile GeoB97-020/027 (Schwenk and Speiss, 2009) running along 8°N over the DSDP site 218 depicts prominent reflectors such as the regional Pleistocene and Pliocene unconformities. The Eocene unconformity was identified further east, on the Ninetyeast Ridge. IODP Leg 354 drilled 7 sites (1449-1455) along 8°N in 2015, to better understand the depositional history of the Bengal Fan. Site U1455 was the reoccupation of site 218 (France-Lanord et al., 2016). It penetrated 942 m to reach sediments of age around 12 Ma. It confirmed the Pleistocene and Pliocene unconformities, and helped to infer other major reflectors such as top of Pliocene, top of Miocene and Miocene unconformity (Table 1).

ODP Leg 116 sites 717, 718 and 719 were drilled to obtain a complete fan record since the lower Miocene (Table 1) near the equator (Cochran et al., 1990). The inferred lithology comprises five units of varying deposits including turbidites, from Recent to Lower Miocene age (Shipboard Scientific party, 1989). Seismic records around the sites facilitated in tracing major unconformities A and B (Cochran et al., 1990). The A unconformity divides the sediments into the pre-deformation and syn-deformation units, and represents the onset of deformation at around 8 Ma. Furthermore, it is a structural unconformity and does not correspond to a change in nature of sediments (Curry and Munasinghe, 1989; Shipboard Scientific party, 1989). The B unconformity runs sub-parallel to the seabed and onlaps the uplifted sediments. The older unconformity at lower Eocene time is not prominent at these sites (Curry and Munasinghe, 1989).

An additional unconformity AA (Table 1) was identified based on seismic records in the eastern Indian Ocean (Krishna et al., 1998). This unconformity coincides with the base of sublithologic unit IVA at the ODP sites 717 and 719. The AA unconformity is seen prevalent in the northern region of

deformation, while the A unconformity was mostly inferred south of 1°S. The B unconformity was observed in the central region (Krishna et al., 2001).

Two major unconformities R1 and R2 (Table 1) were inferred based on a multichannel seismic and OBS profile AWI-20170400 in the CIOB (Altenbernd et al., 2020). The R1 unconformity separates the pre-deformational from the syn-deformational sediments, and is the same as the A unconformity (Curry and Munasinghe, 1989). The younger R2 unconformity lies within the syn-deformational sediments overlapping the older deposits (Altenbernd et al., 2020), and is equivalent to the B unconformity. Furthermore, the entire sediment load was divided into 4 sequences, sed1 (above R1) to sed4 (oldest).

### **3. Data and Methodology**

A 1300 km long geophysical transect SK101 was collected during the 101st cruise of ORV Sagar Kanya in 1995 (Fig. 2). Gravity, magnetic and bathymetry data were collected along with high quality multichannel seismic data. Navigation was done using the Magnavox series 5000 Integrated Navigation System (INS) and Global Positioning System receiver (GPS, Model MX4400). Bathymetric data were obtained using Honeywell Elac deep sea echosounder and gravity data were collected using the KSS30 model sea gravimeter. The Earth's total magnetic intensity data were recorded continuously using Geometric Proton Precession Magnetometer (EG&G Model G801/3).

Multichannel seismic reflection data were acquired using the DFS V system. D-type array of 7 airguns (495 cu inch with 7.9 litre volume) was used as the source, and 24 channel hydrophone streamer with 32 hydrophones per group was used as a signal receiving unit. The group interval was 25 m and the shot interval was 50 m. The sampling rate was 4 msec and the record length was 12 sec. A six fold coverage was achieved using this configuration.

The standard procedures were applied for the reduction of the gravity and magnetic data. Likewise, standard processing techniques were used to obtain the final stack sections of the seismic data. These include demultiplexing, geometry, filtering, deconvolution, nmo correction, velocity analysis and CDP stacking. All processed data sets were integrated (Figs. 3-7 & 8a) to infer the structure and evolutionary history of the subsurface along the transect.

The seismic transect SK101 was divided into 5 sections during the processing stage as shown in different colours in figure 2b. Their names and endpoint shot numbers are as follows: (A) 65-7464, (B) 1-5857, (C) 400-5113, (D) 5116-10000, and (E) 1-5274. Their un-interpreted and interpreted seismic records are provided in figures 3-7. Initially the transect runs from north to south, but at shot 3800 of section A, it turns to run southwest (Fig. 2b). The transect obliquely crosses the N-S trending

86°E FZ (Fig. 2a), which is a broad feature depicting double limbed gravity signature (Wessel et al., 2015). Furthermore, the transect runs over the southern ends of the NW-SE trending FZs, and ends at the ODP site 718.

The northern end of our transect (shot 1530 of section A, Figs. 2b & 3) crosses the profile GeoB97-020/027 (Schwenk and Speiss, 2009). This end also lies around the DSDP218/IODP Leg 354 sites (Von der Borch et al., 1974; France-Lanord et al., 2016). Our transect actually lies between IODP drill sites 1452 and 1453. But both these cores penetrated 215 m into the Early Pleistocene and terminated at 5.2 sec TWT. Hence we have tied our data with the DSDP218 and its overlying site 1455 reaching to 6.08 sec TWT.

The southern endpoint of the transect lies over the ODP Leg 116 sites 717-719 (Shipboard Scientific party, 1989). Here too, we have used the deepest drill site 718 which drilled sediments of age up to 17 Ma (Figs. 2b & 7). This drill site lies at shot 5190 of section E and reaches up to 7.28 sec TWT.

Prominent seismic reflectors/horizons were traced visually based on their characteristic reflection pattern, amplitude and continuity (Figs. 3-7). These horizons were traced along the entire transect despite the interruptions by the basement highs. The horizons inferred from either end of the transect were matched and identified (Fig. 8b, Table 1) using published drill and seismic information (Von der Borch et al., 1974; Cochran, 1990; Murthy et al., 1993; Schwenk and Speiss, 2009; France-Lanord et al., 2016; Altenbernd et al., 2020).

The basement reflector was also studied in detail to define its different characteristics (Figs. 3-9). The seismic records were examined for deformation signatures in the sedimentary column and basement. Deformation signatures such as faults, folds and flower structures were interpreted qualitatively only, due to the oblique azimuth of this single transect with respect to the direction of compressional stress. Furthermore, the earthquake locations (USGS, 2020) were used to correlate the present day seismicity with the deformation activity.

The time sections (Figs. 3-7) were converted to depth sections in order to estimate the sediment thickness in kilometres (Fig. 8c). The interval velocities obtained from the velocity analysis of the multichannel seismic data were used after validating with the published velocities (Naini and Leyden, 1973; Bull and Scrutton, 1990b; Altenbernd et al., 2020). For this exercise, we divided our transect into three parts (northern, central and southern) based on the locations of published seismic velocities (Table 2; Fig. 2b). Velocity information provided by sonobuoy station 264 (Naini and Leyden, 1973) was used to validate the velocities for the northern part of the transect. Velocities obtained from the OBS data (Altenbernd et al., 2020) and wide angle reflection data (Bull and Scrutton, 1990b) were



used for the central and southern portions of the transect respectively. The estimated sediment thickness values (Fig. 8c) were then used to compute the sediment load correction as demonstrated by Sykes (1996). The corrected basement depths were then used to estimate the crustal ages (Parsons and Sclater, 1977).

Our transect was plotted on the 80 Ma plate reconstruction model (Matthews et al., 2016) using Gplates software (Boyden et al., 2011) to understand the evolution of the basement underlying the transect (Fig. 10).

## **4. Results**

### *4.1 Geophysical signatures*

Bathymetry is fairly smooth and increases from the northeast towards southwest, along the transect (Fig. 8a). A 13 km wide double limbed channel (also seen between shots 780-1130 in section A, figure 3) has a highly asymmetric northern limb and a relatively shallow, symmetric southern limb. This channel belongs to the abandoned channel E4 (Curry et al., 2003).

A few prominent topographic highs are seen along the transect (Fig. 8a). P1 is 15 km wide, 545 m high (between shots 2000-2300 in section B, Fig. 4), and P2 is 14 km wide, 682 m high (between shots 700-1020 in section C, Fig. 5). A larger high 'PD' having pedestal like structures on its either side (Fig. 8a) is a 74 km wide structure rising from 3864 m to 3290 m (between shots 2500-3700 in section B, Fig. 4). Two topographic features T1 and T2 seen further southwest, are broader and shallower (Fig. 8a). T1 is 68 km wide and 318 m high (between shots 7900-9700 in section D, Fig. 6), while T2 is 38 km wide and 238 m high (between shots 3000-3500 in section E, Fig. 7).

Free-air gravity appears undulating and broadly mimics the basement with a pronounced gravity low (-75 mgal) between 780 and 900 km (Fig. 8a). Subdued magnetic anomalies are seen between 780 and 1080 km (Fig. 8a), even on the topographic high T1. Furthermore, magnetic anomaly A34 is identified at both ends of our transect.

### *4.2 Subsurface characteristics*

The seismic records (Figs. 3-7) depict a variable sedimentary load having several prominent horizons, and the underlying basement. The sedimentary units are mostly semi-continuous to discontinuous, parallel to sub-parallel reflectors of medium to low amplitude. Five major horizons (H1 to H5) identified using published drilling and seismic results (Table 1) divide the sediment load into six seismic sequences (sed1 to sed6) of variable thickness (Figs. 3-7 & 8b). In general, the lowermost sequence sed1 is of low amplitude (transparent), and the horizon H5 is sub-parallel to the seabed.

The basement reflector can be plainly identified except towards north and over the 86°E FZ (Figs. 3-7). Nevertheless, we consider the basement as acoustic basement and henceforth, by the word 'basement' we mean 'acoustic basement'. No crustal information could be retrieved below the basement, which is frequently faulted. The basement and sediments are relatively less faulted/folded towards northeast along the transect (Figs. 3-5), in comparison with that observed towards southwest (Figs. 6-7). Near vertical faults associated with branch faults are also seen randomly at different depths, along the transect. These faults are frequent in the vicinity of fracture zones and appear as flower/half flower structures (Figs. 3-6).

Section A (shots: 65-7464) depicts thick sediment load (up to 3 sec TWT) at the northern end of the transect (Fig. 3a). The lower sequences sed1 to sed4 maintain their thickness throughout the section, while sed5 thins towards southwest consistent with recent sediment supply from the north. At shot 3500, the basement is faulted forming a flower structure within the overlying sediments which are folded up to ~0.2 sec TWT (Fig. 3b). In the 86°E FZ area, the sediment layers sed1 to sed4 are folded (up to 0.3 sec TWT) and offset by asymmetrical flower structures, depicting minor compression (Fig. 9a).

Section B (shots: 1-5857) depicts a broad complex structure (shots 1400 to 5400) of protruding highs (P1 and PD) and a buried high (shots 4800 to 5200), with older sediments terminating at their flanks (Fig. 4a). Along this section, deformation signatures such as folding of the entire sediment column on either side of the basement high PD (Fig. 4b), and earthquake activity suggest that deformation is continuing till date.

Section C (shots: 400-5113) depicts a protruding high (P2) and a buried basement high beyond which the basement runs deep up to 8.8 sec TWT with a significant 3 sec TWT sediment load (Fig. 5a). A prominent horizontal layer akin to basement at 8.6 sec TWT (Fig. 9b) illustrates that the basement high may have emplaced by piercing through the original horizontal basement. Two episodes of gentle folding with near vertical faults/half flower structures in the older sediment load and basement can be inferred southwest of the basement highs (Fig. 5b). The first episode has occurred after sed3 was deposited, while mild folding of sequence sed4 suggests the occurrence of the second episode.

Section D (shots: 5116-10000) depicts minor long wavelength folding of the lower sedimentary strata and basement towards southwest (Fig. 6a). This folding has resulted in the low amplitude deformational high T1 characterised with heavy faulting/flower structures in the upper strata (Fig. 6b). The uneven seabed and earthquake activity suggests continuation of deformation activity till date. The

basement beneath the high is undulatory with a ~0.3 sec TWT layer seen within the troughs (Figs. 6b & 9c).

Section E (shots: 1-5274, right to left in figure 7) depicts intense faulting and folding of the basement and the older strata. Furthermore, asymmetrical folding and high-angle reverse faulting have formed the deformational high T2 flanked by shallow basins on its either side (Fig. 7b). In the northeastern basin, older sequences sed1 to sed3 are deformed while in the southwestern basin, sequence sed4 is deformed too. Faulting/folding at the seabed and earthquake activity suggest that deformation is ongoing within the deformational high T2. A significant step in basement is seen at shot 471, with the basement abruptly rising from 8.4 to 8 sec TWT while the horizon H1 is nearly flat (Fig. 9d).

#### *4.3 Estimated crustal ages*

The interval velocities used for computation of sediment thickness vary along the profile (Table 2). The velocities are higher at sonobuoy station 264 (Naini and Leyden, 1973) in comparison to those reported towards southwest (Bull and Scrutton, 1990b; Altenbernd et al., 2020). The computed sediment thickness in general varies between 2 and 4 km (Fig. 8c). The thickness is minimal (<0.1 km) over the basement highs and reaches up to 4.5 km towards north as well as in the deep basement area. The sediment corrected depths range between 3.5 and 6.0 km, and may not be accurate over the basement highs. The estimated crustal ages (Fig. 8c) are highly sensitive to the undulations in the sediment corrected depths as well as strike-slip faulting. The computed ages are in the range of 60-80 Ma towards north. Higher crustal ages (140-160 Ma) are inferred in the deep basement region. Further southwest, the estimated crustal ages range between 80 to 100 Ma. An age difference of at least 10 Ma can be inferred at the step in basement.

The plate model depicts that the crust beneath the entire transect has evolved by 80 Ma (Fig. 10) and the crustal age does not exceed 108 Ma. The step in the basement lies on the plate boundary inferred at 100 Ma (Matthews et al., 2016). Limited crust is seen on the Indian plate in comparison to the Antarctica plate (between 100 and 83 Ma), in the spreading corridor south of the basement step. . Furthermore, the 86°E FZ is seen as the southward continuation of the 85°E Ridge.

### **5. Discussion**

The potential field data together with multichannel seismic data along our transect SK101 reveal several important characteristics of the subsurface. The gravity signature varies independent of the topography but is influenced by the basement configuration (Fig. 8). The 86°E FZ (between 320 and 420 km in figure 8a) depicts low gravity as seen over fracture zones worldwide (Louden and Forsyth, 1982; White et al., 1984).

The presence of magnetic anomaly A34 in the vicinity of the endpoints of our transect suggests that the surrounding crust is of Late Cretaceous age (Fig. 2a). The oceanic crust in the eastern basin of the Bay of Bengal is of Middle Cretaceous age (Desa and Ramana, 2016), hence our northern endpoint probably lies on oceanic crust of age ~87 Ma. Our southern endpoint lies south of A34 anomaly hence its crustal age may be around 81 Ma (Desa et al., 2019). The estimated crustal ages (60-80 Ma) towards north are lower than expected, and this could be because the actual basement may be deeper than our inferred acoustic basement (Figs. 3 & 8b). Towards the southern end of our transect, the computed ages range between 80-100 Ma and are within the expected range.

The conspicuous low amplitude-low frequency magnetic field (780-1080 km, Fig. 8a) endorses the fact that the underlying crust is of Middle Cretaceous age (83-120 Ma) associated with largely normal and smooth geomagnetic field (Tarduno et al., 2001). Furthermore, the plate reconstruction model (Fig. 10) depicts that most of our profile lies within the Middle Cretaceous period, more specifically, between 100 and 108 Ma. But our computed crustal ages are higher in the deep basement region, i.e. 140 to 160 Ma (780-900 km in figure 8c), and can be attributed to its abnormally deep basement (~8.8 sec TWT) probably caused by subsequent lithospheric flexure as proposed by Altenbernd et al. (2020). We thus consider the higher ages to be erroneous and stick to our interpretation that the deep basement region is of Middle Cretaceous age.

The presence of a thick sediment load of 4.5 km in the deep basement region (780-900 km in figure 8c) was rather unexpected considering its location far from any significant sediment source. Similar sediment thickness (~5 km) has been reported in this region (Altenbernd et al., 2020). This sediment load comprises ~1.5 km thick lowermost sequence sed1 (Table 2), considered as pre-fan sediments by Murthy et al. (1993). We suspect that the adjoining basement highs (Figs. 2 & 8) may have played a major role in the rapid accumulation of the older sediments in this region.

The prominent step in the basement (0.4 sec TWT, ~800 m, Fig. 9d) depicting a significant change in the magnetic anomaly pattern (Fig. 8a) and age offset of about 10 Ma (Fig. 8c), suggests the concurrent presence of oceanic crust of different ages at this location. It indicates that the basement step denotes a plate boundary such as a fracture zone or a ridge jump. The basement step is located ~50 km southwest of the NW-SE trending fracture zone (Fig. 10), and hence may not be an offsetting fault in a flower structure over the fracture zone. Rather, the step may manifest lack of continuous crust due to a ridge jump. Northward ridge jumps have been postulated to occur in this region (Rotstein et al., 2001) leaving excess crust and an extinct spreading center (Nogi et al., 2004) on the Antarctica plate. Indeed, the location of the basement step along the 100 Ma plate boundary, and excess crust on the

Antarctica plate in the related spreading corridor between 100 and 83 Ma suggests it could be a ridge jump associated with the Middle Cretaceous major plate reorganization (Fig. 10).

### *5.1 Deformation signatures*

Our profile lies in the CIOB deformation zone (Fig. 2), where shortening has taken place in the form of east-west striking folds and reverse faults in the sedimentary load and basement (Weissel et al., 1980; Geller et al., 1983, Chamot-Rooke et al., 1993). The seismic record illustrates that deformation is relatively mild towards north and intense towards south in the study area. Furthermore, one can see the occurrence of three discrete deformation episodes (8 Ma, 4 Ma and 0.8 Ma), in agreement to those reported by Krishna et al. (1998).

The deformation pattern southwest of the basement rise P2 in sections C to E (Figs. 5-7 & 8b) suggests that the first deformation episode took place after the deposition of sequence sed3 i.e. Upper Miocene time. This episode gave rise to a huge basin/syncline (deep basement region) and a broad anticline T1 (Figs. 5-6) belonging to the long wavelength-low amplitude folding (Weissel et al., 1980; Neprochnov et al., 1988). Furthermore, the deformational high T2 (Fig. 7) belongs to the narrow asymmetric folding, high-angle reverse faulting caused by reactivation of the pre-existing spreading center related fault fabric (Bull and Scrutton, 1990a).

The second episode of deformation of Pliocene age (folding of horizon H4) is seen as a mild event in the deep basement region (Fig. 5) but as an intense event south of the topographic high T2 (Fig. 7). It is also seen further north on the eastern edge of the 86°E FZ as a prominent 0.3 sec TWT folding of the sequences sed1 to sed4 (Figs. 3 & 9a).

The folding of the horizon H5 on either side of the basement high PD (Fig. 4), and faulting of the horizons H2 to H5 (shot 3730) suggests the occurrence of the third deformation episode at Pleistocene time. The undulations on the seabed and seismicity are indicators of continuation of deformation activity till date. Furthermore, the earthquake epicenters lie around topographic highs on our transect (Figs. 3-7) in agreement to the proposition that stress is released at such highs through seismicity (Levchenko, 1992).

The flower structures seen along the entire transect (Figs. 3-7) range from near symmetrical with (shot 3500, Fig. 3) to highly asymmetrical (shot 4000, Fig. 5). Similar structures seen in the northwestern Wharton Basin are considered as strike-slip events (Stevens et al., 2020). This observation is interesting since very few strike-slip earthquakes have been reported in the southern Bay of Bengal, most earthquakes depicting thrust faulting (Bergman and Solomon, 1980). Furthermore, near vertical faults/flower structures are more prevalent over fracture zones such as the 86°E FZ (Figs. 3 & 9a).

Heavy faulting/flower structures in the upper strata and prominent undulations in the basement are also seen within the deformational high T1 (Figs. 6 & 9c) which overlies the NW-SE trending fracture zone (Fig. 2b). Similar features are observed over fracture zones worldwide (e.g. Geletti et al., 2005), and indicate strike-slip activity and/or partial reactivation of the pre-existing faults (Harding, 1985). Moreover, these features support the fact that fracture zones are structurally weak (Bonneville and McNutt, 1992), and hence more susceptible to deformation activity as observed by Krishna et al. (1998).

Our transect suggests that Pliocene and Pleistocene deformation occurred towards north in agreement with the spatial extent demarcated by Krishna et al. (2001). Furthermore, Miocene deformation seen on our transect is in contrast to the conclusion of Krishna et al. (2001) that Miocene activity occurred south of the ODP Leg 116 sites.

### *5.2 Arcuate gravity low*

Satellite gravity suggests that the arcuate shaped gravity low seen southeast of Sri Lanka (Fig. 2) can be linked to the 85°E Ridge, as postulated by Curray and Munasinghe (1991) and Muller et al. (1993). In contrast, Altenbernd et al. (2020) concluded that the southwest trending gravity low is due to a flexural basin of normal oceanic crust caused by mid-Miocene or younger compressional intraplate lithospheric deformation. Furthermore, they stressed that the flexural basin and its gravity anomaly are much younger than the 85°E Ridge and the ANS.

In the present study, this gravity low (-75 mgal) is seen south of the basement highs (south of 5°N). It is associated with the deep basement (~8.8 sec TWT) and subdued magnetic anomalies (Fig. 8a, 780-900 km). This deep basement is of Middle Cretaceous age and is overlain by ~3 sec TWT thick sediments (Fig. 8b). Moreover, this region is affected by two episodes of deformation forming a huge syncline with ~0.8 sec TWT flexure. The presence of the basement highs towards north and the anticline formed by deformation towards south adds to the dimensions of this deep basement enhancing the gravity low.

The trend of the arcuate gravity low is similar to the NE-SW trend of the Early Cretaceous spreading center in this region (Fig. 2a). Thus, this low must have formed due to deformation along the pre-existing seafloor spreading related faulting fabric, as suggested by Bull and Scrutton (1990a). Further the basement highs lying to its north (Fig. 2b) may have blocked the northward propagation of compression resulting in a more pronounced flexure. So, we are in agreement with Altenbernd et al. (2020) that the arcuate gravity low is due to a deep, old and sediment filled flexural basin caused by

deformation. We are also of the opinion that the low is not related to the 85°E Ridge, in contrast to the link proposed by Curray and Munasinghe (1991) and Muller et al. (1993).

### *5.3 Topographic highs*

The topographic highs identified in this study (Figs. 3-8) range from relatively steep basement highs towards northeast to broad oval-circular deformational rises towards southwest. The basement highs lying at the southern end of the NW-SE trending Early Cretaceous fracture zones and in close proximity to the N-S trending 86°E FZ, terminate the oldest sediments at their flanks suggesting that these highs have existed prior to the sediment deposition (Figs. 3-5 & 8b). The presence of a discontinuous horizontal basement reflector below the basement high suggests that the high may have emplaced extrusively by piercing the original basement (Fig. 9b) and is akin to a volcanic knoll (e.g. Tsuru et al., 2008). Similar basement highs of nondeformational origin were reported around 1°S and 84°E (Levchenko, 1992), and proposed to be volcanic structures developed near the intersection of a transform fault with the mid-ocean ridge axis at the end of Cretaceous –early Paleocene (Kashintsev et al., 1987). We suspect that the steep highs inferred in the present study may have been similarly emplaced in a nondeformational tectonic setup. Furthermore, these highs are not related to the 85°E Ridge, in contrast to that proposed by Krishna (2003).

The moderate topographic highs noticed towards southwest (T1 and T2, beyond 1000 km in figure 8) have a deformational origin (Figs. 6-7). They belong to the two scales of deformation (Neprochnov et al., 1988, Bull and Scrutton, 1990a). The deformational high T2 is narrow with intense asymmetric folding and closely spaced high-angle reverse faulting. In contrast, the deformational high T1 is broad, with uneven seabed due to heavy faulting/flower structures in the upper strata. The undulatory acoustic basement with a 0.3 sec TWT layer above it probably indicates the occurrence of intrusive volcanism before sediment deposition. Thus, the high T1 (Figs. 6 & 9c) has formed over the NW-SE trending fracture zone (Fig. 2b), a conducive locus for release of thermal and compressional stress.

### *5.4 Tectonic evolution*

NW-SE trending crustal accretion in the western basin of the Bay of Bengal and south of Sri Lanka, and conjugate western Enderby Basin, East Antarctica, persisted until 108 Ma (Fig. 10) (Matthews et al., 2016). The 86°E/Kerguelen FZ became active after 108 Ma, with the older NW-SE trending fracture zones truncating against it. Furthermore, the seafloor spreading between India and Antarctica became N-S by 100 Ma with a clockwise rotation of the NW-SE trending transform faults.

This rotation resulted in horizontal compression (McCarthy et al., 1996) fracturing the lithosphere, and subsequent post transform volcanism may have caused the formation of the nondeformational

basement highs as observed by Caress et al. (1988) elsewhere. These tectonics are substantiated by the presence of an abruptly terminating horizontal basement reflector below the basement highs (Fig. 9b).

Asymmetric spreading occurred between India and Antarctica during the Middle Cretaceous generating excess crust on the Antarctica plate (Fig. 10). This asymmetry has been attributed to northward ridge jumps by Rotstein et al. (2001) and Nogi et al. (2004), resulting in concurrent presence of oceanic crust of different ages. The step in basement coinciding with a significant change in the magnetic anomaly pattern (Fig. 8) probably belongs to the 100 Ma plate boundary (northward ridge jump, Fig. 10) associated with the global major plate reorganization during the Middle Cretaceous period (Matthews et al., 2012).

### **Conclusions**

Integrated analysis of geophysical data suggests that the transect SK101 is underlain by Middle to Late Cretaceous crust. Gravity signature along the transect is influenced by the basement configuration.

The sediment thickness is about 3 sec TWT in the north and in the deep basement region. Five prominent horizons have been traced in the sedimentary column and identified as Pleistocene, Pliocene, Miocene and Eocene unconformities and 12 Ma. Deformation signatures such as folding/faulting/flower structures are seen along the transect, and are more pronounced over fracture zones and towards south.

The basement highs lying at the southern end of the NW-SE trending fracture zones may have formed as the spreading ridge rotated clockwise during the Middle Cretaceous fracturing the lithosphere and subsequent post transform volcanism. The arcuate gravity low has formed due to the presence of a deep (8.8 sec TWT) and old (Middle Cretaceous age) basement with thick (~3 sec TWT) sediment load.

A step in the basement coinciding with a significant change in magnetic anomaly pattern probably indicates the concurrent presence of oceanic crust of different ages at this location. This feature may be a part of the 100 Ma plate boundary associated with the Middle Cretaceous major plate reorganisation.

### **Acknowledgements**

Director, NIO is thanked for granting ship time and the necessary permission. The scientists and technical staff of the 101<sup>st</sup> cruise of ORV Sagar Kanya are acknowledged for their help in data acquisition. We thank Dr. W. Jokat and Dr. B. Davy for their constructive reviews. CSIR-NGRI is



acknowledged for assisting in processing the seismic data. Figures are generated using GMT software (Wessel and Smith, 1998). This is CSIR-NIO contribution

## References

- Altenbernd, T., Jokat, W., Geissler, W., 2020. The bent prolongation of the 85°E Ridge south of 5°N – Fact or fiction? *Tectonophysics* <https://doi.org/10.1016/j.tecto.2020.228457>.
- Anand, S.P., Rajaram, M., Majumdar, T.J., Bhattacharya, R., 2009. Structure and tectonics of 85°E Ridge from analysis of geopotential data. *Tectonophysics* 478, 100-110.
- Bastia, R., Radhakrishna, M., Srinivas, T., Nayak, S., Nathaniel, D.M., Biswal, T.K., 2010. Structural and tectonic interpretation of geophysical data along the Eastern Continental Margin of India with special reference to the deep water petroliferous basins. *J. Asian Earth Sci.* 39, 608–619.
- Bergman, E.A., Solomon, S.C., 1980. Oceanic intraplate earthquakes implications for local and regional intraplate stress. *J. Geophys. Res.* 85, 5389-5410.
- Bernard, A., Munsch, M., Rotstein, Y., Sauter, D., 2005. Refined spreading history at the Southwest Indian Ridge for the last 96 Ma, with the aid of satellite gravity data. *Geophys. J. Int.* 162, 765-778.
- Bonneville, A., McNutt, M., 1992. Shear strength of the great Pacific fracture zones. *Geophys. Res. Lett.* 19, 2023-2026.
- Boyden, J. A., Müller, R. D., Gurnis, M., Torsvik, T. H., Clark, J. A., Turner, M., Ivey-Law, H., Watson, R. J., Cannon, J. S., 2011. Next generation Plate-tectonic Reconstructions Using GPlates. In: Keller, G. R., Baru, C. (Eds.), *Geoinformatics: Cyberinfrastructure for the Solid Earth Sciences*. Cambridge University Press, Cambridge, UK, pp. 95–113.
- Bull, J.M., Scrutton, R.A., 1990a. Fault reactivation in the Central Indian Ocean and the rheology of oceanic lithosphere. *Nature* 344, 855-858.
- Bull, J.M., Scrutton, R.A., 1990b. Sediment velocities and deep structure from wide-angle reflection data around Leg 116 sites. In: Cochran J.R. et al., (Eds.), *Proc. ODP, Sci. Res.* 116, pp. 311-316.
- Caress, D.W., Menard, H.W., Hey, R.N., 1988. Eocene reorganization of the Pacific-Farallon spreading center north of the Mendocino fracture zone. *J. Geophys. Res.* 93, 2813-2838.
- Chamot-Rooke, N., Jestin, F., de Voogd, B., Phedre working group, 1993. Intraplate shortening in the central Indian Ocean determined from a 2100-km-long north-south deep seismic reflection profile. *Geology* 21, 1043-1046.
- Cochran, J.R., 1990. Himalayan uplift, sea level, and the record of Bengal fan sedimentation at the ODP Leg 116 sites. In: Cochran J.R. et al., (Eds.), *Proc. ODP, Sci. Res.* 116, pp. 397-414.

- Curry, J. R., 1994. Sediment volume and mass beneath the Bay of Bengal, *Earth Planet. Sci. Lett.* 125, 371-383.
- Curry, J. R., Emmel, F. J., Moore, D. G., Raitt, R. W., 1982. Structure, tectonics and geological history of the Northeastern Indian Ocean. In: Nairn, A. E., Stehli, F. G. (Eds.) *The Ocean Basins and Margins* 6, Plenum, New York, pp. 399-450.
- Curry, J. R., Munasinghe, T., 1989. Timing of intraplate deformation, northeastern Indian Ocean. *Earth Planet. Sci. Lett.* 94, 71-77.
- Curry, J. R., Munasinghe, T., 1991. Origin of the Rajmahal Traps and the 85°E Ridge: Preliminary reconstructions of the Crozet hotspot. *Geology* 19, 1237-1240.
- Curry J. R., Emmel, F. J., Moore, D. G., 2003. The Bengal Fan: morphology, geometry, stratigraphy, history and processes. *Mar. Petr. Geol.* 19, 1191-1223.
- Delescluse, M., Montesi, L.G.J., Chamot-Rooke, N., 2008. Fault reactivation and selective abandonment in the oceanic lithosphere. *Geophys. Res. Lett.* 35, L16312, doi:10.1029/2008GL035066.
- Deplus, C., Diament, M., Hébert, H., Bertrand, G., Dominguez, S., Dubois, J., Malod, J., Patriat, P., Pontoise, B., Sibilla, J.J., 1998. Direct evidence of active deformation in the eastern Indian Oceanic plate. *Geology* 26, 131-134.
- Desa, M., Ramana, M. V., Ramprasad, T., 2006. Seafloor spreading magnetic anomalies south off Sri Lanka. *Mar. Geol.* 229, 227-240.
- Desa, M., Ramana, M. V., Ramprasad, T., 2009. Evolution of the Late Cretaceous crust in the equatorial region of the Northern Indian Ocean and its implication in understanding the plate kinematics. *Geophys. J. Int.* 177, 1265-1278.
- Desa, M., Ramana, M. V., Ramprasad, T., Lall, M. V., Kumar, B.J.P., 2013. Geophysical signatures over and around the northern segment of the 85°E Ridge, Mahanadi offshore, Eastern Continental margin of India: Tectonic implications. *J. Asian Earth Sci.* 73, 460-472.
- Desa, M., Ramana, M. V., 2016. Middle Cretaceous geomagnetic field anomalies in the Eastern Indian Ocean and their implication to the tectonic evolution of the Bay of Bengal, *Mar. Geol.* 382, 111–121.
- Desa, M., Ismaiel, M., Suresh, Y., Krishna, K.S., 2018. Oblique strike-slip motion off the Southeastern Continental Margin of India: Implication for the separation of Sri Lanka from India. *J. Asian Earth Sci.* 156, 111-121.
- Desa, M., Ramprasad, T., Kamesh Raju, K.A., 2019. An integrated geophysical study east of the southern Chagos Laccadive Ridge Complex, Central Indian Ocean Basin: Implications for the Rodriguez Triple Junction dynamics in the Late Cretaceous. *Mar. Geol.* 414, 47-63.
- Eldholm, O., Coffin, M.F., 2000. Large igneous provinces and plate tectonics. In: Richards, M.A. et al., (Eds.), *The History and Dynamics of Global Plate Motions*. 121, Geophysical Monograph, American Geophysical Union, Washington, pp. 309–326.

- France-Lanord, C., Spiess, V., et al., 2016. Site U1455. In: France-Lanord, C., Spiess, V., Klaus, A., Schwenk, T., and the Expedition 354 Scientists (Eds.), Bengal Fan. Proceedings of the International Ocean Discovery Program, 354: College Station, TX (International Ocean Discovery Program). <http://dx.doi.org/10.14379/iodp.proc.354.109.2016>.
- Gaina, C., Muller, R.D., Brown, B., Ishihara, T., Ivanov, S., 2007. Breakup and early seafloor spreading between India and Antarctica. *Geophys. J. Int.* 170, 151-169.
- Gee, J.S., Kent, D.V., 2007. Source of oceanic magnetic anomalies and the geomagnetic polarity timescale. *Treatise on Geophysics* 5, 455-507.
- Geletti, R., Lodolo, E., Schreider, A.A., Polonia, A., 2005. Seismic structure and tectonics of the Shackleton Fracture Zone (Drake Passage, Scotia Sea). *Mar. Geophys. Res.* 26, 17-28.
- Geller, C.A., Weissel, J.K., Anderson, R.N., 1983. Heat transfer and intraplate deformation in the central Indian Ocean. *J. Geophys. Res.* 88, 5560-5570.
- Gibbons, A.D., Whittaker, J.M., Muller, R.D., 2013. The breakup of East Gondwana: Assimilating constraints from Cretaceous ocean basins around India into a best-fit tectonic model. *J. Geophys. Res.* 118, 1–15.
- Gopala Rao, D., Krishna, K.S., Sar, D., 1997. Crustal evolution and sedimentation history of the Bay of Bengal since the Cretaceous. *J. Geophys. Res.* 102, 17747-17768.
- Gordon, R.G., DeMets, C., Royer, J-Y., 1998. Evidence for long-term diffuse deformation of the lithosphere of the equatorial Indian Ocean. *Nature* 395, 370-373.
- Goslin, J., Schlich, R., 1982. Structural limits of the South Crozet Basin –Relations to Enderby Basin and the Kerguelen-Heard Plateau. In: Craddock, C., Loveless, J.K., Vierima, T.L., Crawford, K. (Eds.), *Antarctica Geoscience*. University of Wisconsin Press, Madison, WI. pp. 79–85.
- Granot, R., Dyment, J., Gallet, Y., 2012. Geomagnetic field variability during the Cretaceous Normal Superchron. *Nat. Geosci.* 5, 220–223. <http://dx.doi.org/10.1038/ngeo1404>.
- Harding, T.P., 1985. Seismic characteristics and identification of negative flower structures, positive flower structures, and positive structural inversion. *Amer. Ass. Pet. Geol. Bull.* 69, 585-600.
- Heezen, B.C., Tharp, M., 1964. *Physiographic Diagram of the Indian Ocean (With Descriptive Sheet)*. Geological Society of America, New York.
- Kashintsev, G. L., Pyeve, A.A., Rudnik, G.B., 1987. Subbalkalic volcanism in the Central basin of the Indian Ocean. *Izv. Akad. Nauk. SSR, Ser. Geol.* 2, 42-49.
- Kent, R., 1991. Lithospheric uplift in eastern Gondwana: Evidence for a long-lived mantle plume system? *Geology* 19, 19–23.
- Kent, R. W., Storey, M., Saunders, A. D., Ghose, N. C., Kempton, P. D., 1992. Comments and reply on “Origin of the Rajmahal Traps and the 85°E Ridge: Preliminary reconstructions of the trace of the Crozet hotspot. *Geology* 20, 957-958.

- Kent, R.W., Pringle, M.S., Müller, R.D., Saunders, A.D., Ghose N.C., 2002.  $^{40}\text{Ar}/^{39}\text{Ar}$  geochronology of the Rajmahal basalts, India, and their relationship to the Kerguelen Plateau. *J. Petrol.* 43, 1141-1153.
- Krishna, K.S., 2003. Structure and evolution of the Afanasy Nikitin seamount, buried hills and 85°E Ridge in the northeastern Indian Ocean. *Earth Planet. Sci. Lett.* 209, 379–394. doi:10.1016/S0012-821X(03)00081-5.
- Krishna, K.S., Ramana, M.V. Gopala Rao, D., Murthy, K.S.R., Malleswara Rao, M.M., Subrahmanyam, V., Sarma, K.V.L.N.S., 1998. Periodic deformation of oceanic crust in the Central Indian Ocean. *J. Geophys. Res.* 103, 17859-17875.
- Krishna, K.S., Bull, J.M., Scrutton, R.A., 2001. Evidence for multiphase folding of the Central Indian Ocean lithosphere. *Geology* 29, 715-718.
- Klootwijk, C.T., Gee, J.S., Pierce, J.W., Smith, G.M., 1992. The origin of Ninetyeast Ridge: paleomagnetic constraints from ODP Leg 121. *J. Southeast Asian Earth Sci.* 7, 247-252.
- Levchenko, O.V., 1992. Detailed studies of the sedimentary cover in the area of intraplate deformation of the Indian Ocean lithosphere. *Oceanology*, 32, 357-363.
- Liu, C., Sandwell, D.T., Curray, J.R., 1982. The Negative Gravity Field over the 85°E Ridge. *J. Geophys. Res.* 87, 7673–7686. doi:10.1029/JB087iB09p07673.
- Louden, K.E., Forsyth, D.W., 1982. Crustal structure and isostatic compensation near the Kane fracture zone from topography and gravity measurements-I. Spectral analysis approach. *Geophys. J.R. Astr. Soc.* 68, 725-750.
- Matthews, K.J., Seton, M., Muller, R.D., 2012. A global-scale plate reorganization event at 105-100 Ma. *Earth Planet. Sci. Lett.* 355-356, 283-298.
- Matthews, K. J., Maloney, K. T., Zahirovic, S., Williams, S. E., Seton, M., Müller, R. D., 2016. Global plate boundary evolution and kinematics since the late Paleozoic. *Global Planet. Change* doi: 10.1016/j.gloplacha.2016.10.002.
- McCarthy, M.C., Kruse, S.E., Brudzinski, M.R., Ranieri, M.E., 1996. Changes in plate motions and the shape of Pacific fracture zones. *J. Geophys. Res.* 101, 13715-13730.
- Muller, R.D., Royer, J.Y., Lawver, L.A., 1993. Revised plate motions relative to the hotspots from combined Atlantic and Indian Ocean hotspot tracks. *Geology* 21, 275–278. doi:10.1130/0091-7613.
- Murthy, K.S.R., Neprochnov, Y.P., Levchenko, O.V., Rao, T.C.S., Milanovsky, V.E., Lakshminarayana, S., 1993. Some new observations on the intra-plate deformation in the Central Indian Basin (CIB). *Mar. Geol.* 114, 185-193.
- Naini, B.R., Leyden, R., 1973. Ganges Cone: a wide angle seismic reflection and refraction study. *J. Geophys. Res.* 78, 8711-8720.
- Neprochnov, Yu.P., Levchenko, O.V., Merklin, L.V., Sedov, V.V., 1988. The structure and tectonics of the intraplate deformation area in the Indian Ocean. *Tectonophysics* 156, 89-106.

- Nogi Y., Nishi, K., Seama, N., Fukuda, Y., 2004. An interpretation of the seafloor spreading history of the West Enderby Basin between initial breakup of Gondwana and anomaly C34. *Mar. Geophys. Res.* 25, 219-229.
- Parsons, B., Sclater, J.G., 1977. An analysis of the variation of ocean floor bathymetry and heat flow with age. *J. Geophys. Res.* 82, 803-827.
- Pierce, J.W., 1978. The northward motion of India since the Late Cretaceous. *R. Astr. Soc. Geophys. J.* 52, 277-311.
- Powell, C. M., Roots, S. R., Veevers, J. J., 1988. Pre-breakup continental extension in East Gondwanaland and the early opening of the eastern Indian Ocean. *Tectonophysics* 155, 261-283.
- Ramana, M. V., Nair, R. R., Sarma, K. V. L. N. S., Ramprasad, T., Krishna, K. S., Subrahmanyam, V., D'Cruz, M., Subrahmanyam, C., Paul, J., Subrahmanyam, A. S., Chandrasekhar, D. V., 1994. Mesozoic anomalies in the Bay of Bengal. *Earth Planet. Sci. Lett.* 121, 469 - 475.
- Ramana, M. V., Subrahmanyam, V., Sarma, K. V. L. N. S., Desa, M., Malleswara Rao, M. M., Subrahmanyam, C., 1997a. Record of the Cretaceous magnetic quiet zone: A precursor to the understanding of evolutionary history of the Bay of Bengal. *Curr. Sci.* 72, 669-673.
- Ramana, M. V., Subrahmanyam, V., Chaubey, A.K., Ramprasad, T., Sarma, K. V. L. N. S., Krishna, K. S., Desa, M., Murty, G.P.S., 1997b. Structure and origin of the 85°E Ridge. *J. Geophys. Res.* 102, 17995-18012.
- Ramana, M.V., Ramprasad, T., Desa, M., 2001. Seafloor spreading magnetic anomalies in the Enderby Basin, East Antarctica. *Earth Planet Sci. Lett.* 191, 241-255.
- Rotstein, Y., Munsch, M., Bernard, A., 2001. The Kerguelen Province revisited: Additional constraints on the early development of the Southeast Indian Ocean. *Mar. Geophys. Res.* 22, 81-100.
- Royer, J-Y., Coffin, M.F., 1992. Jurassic to Eocene plate tectonic reconstructions in the Kerguelen Plateau region. In: Wise, S.W., Schlich, R., et al., (Eds.), *Proc. Ocean Drilling Program, Sci. Res.* 120, pp. 917-928.
- Sandwell, D.T., Muller, R. D., Smith, W. H. F., Garcia, E., Francis, R., 2014. New global marine gravity model from CryoSat-2 and Jason-1 reveals buried tectonic structure. *Science* 346, 65-67.
- Schwenk, T., Spieb, V., 2009. Architecture and stratigraphy of the Bengal Fan as response to tectonic and climate revealed from high-resolution seismic data. In: Kneller, Martinsen, McCaffrey (Eds.), *External Controls on Deep-Water Depositional Systems* 92, SEPM, pp. 107-131.
- Sclater, J.G., Fisher, R.L., 1974. Evolution of the east Central Indian Ocean with emphasis on the tectonic setting of the Ninetyeast Ridge. *Geol. Soc. Amer. Bull.* 85, 683-702.
- Shipboard Scientific party, 1989. Site 718: Bengal Fan. In: Cochran J.R. et al., (Eds.), *Proc. ODP, Init. Repts.*, 116, College Station, TX, pp. 91-154.
- Smith, W. H. F., Sandwell, D., 1997. Global seafloor topography from satellite altimetry and ship depth soundings. *Science* 277, 1956-1962.

- Stevens, D.E., McNeill, L.C., Henstock, T.J., Delescluse, M., Chamot-Rooke, N., Bull, J.M., 2020. A complete structural model and kinematic history for distributed deformation in the Wharton Basin. *Earth Planet. Sci. Lett.* 538, doi.org/10.1016/j.epsl.2020.116218
- Sykes, T.J.S., 1996. A correction for sediment load upon the ocean floor: Uniform versus varying sediment density estimations-implication for isostatic corrections. *Mar. Geol.* 133, 35-49.
- Talwani, M., Desa, M. A., Ismaiel, M., Krishna, K.S., 2016. The Tectonic Origin of the Bay of Bengal and Bangladesh. *J. Geophys. Res.* 121, 4836–4851, doi:10.1002/2015JB012734.
- Tarduno, J.A., Cottrell, R.D., Smirnov, A.V., 2001. High geomagnetic intensity during the mid Cretaceous from Thellier analyses of single plagioclase crystals. *Science* 291, 1779–1783.
- Tsuru, T., Okuda, A., No, T., Kaneda, Y., Tamaki, K., 2008. 2008. Subsurface structure of the Myojin Knol pumiceous volcano obtained from multichannel seismic reflection data. *Earth Planets Space* 60, 721-726.
- U.S. Geological Survey, 2020, Earthquake Lists, Maps, and Statistics, <https://www.usgs.gov/natural-hazards/earthquake-hazards/lists-maps-and-statistics>
- Von der Borch, C.C., Sclater, J.G., et al., 1974. Initial Reports, DSDP22, Washington (US Govt. Printing Office), 885 pp.
- Weissel, J.K., Anderson, R.N., Geller, C.A., 1980. Deformation of the Indo-Australian plate. *Nature* 287, 284-291.
- Wessel, P., Smith, W. H. F., 1988. New, improved version of the Generic Mapping Tools released. *EOS Trans. AGU* 79, 579.
- Wessel, P., Matthews, K.J., Muller, R.D., Mazzoni, A., Whittaker, J.M., Myhill, R., Chandler, M.T., 2015. Semi automatic fracture zone tracking. *Geochem. Geophys. Geosys.* doi: 10.1002/2015GC005853.
- White, R.S., Detrick, R.S., Sinha, M.C., Cormier, M.H., 1984. Anomalous seismic crustal structure of oceanic fracture zones. *Geophys. J.R. Astr. Soc.* 79, 779-798.
- Wiens, D.A., DeMets, C., Gordon, R.G., Stein, S., Argus, D., Engeln, J.F., Lundgren, P., Quible, D., Stein, C., Weinstein, S., Woods, D.F., 1985. A diffuse plate boundary model for Indian Ocean tectonics. *Geophys. Res. Lett.* 12, 429-432.

## Figure captions

Fig. 1: Predicted bathymetry map of the Indian Ocean (version 18.1; Smith and Sandwell, 1997). Fracture zones are marked as dashed black lines (Wessel et al., 2015). Large igneous provinces are marked as thin red outlines (Eldholm and Coffin, 2000). The Indian mid-ocean ridge system is marked in blue. The extent of deformation is shown in dashed orange outline (Gordon et al., 1998). Study area is shown in a black box with red squares denoting the DSDP/ODP sites. 86FZ: 86°E FZ; A: Andaman Sea; AS: Arabian Sea; BR: Broken Ridge; CB: Crozet Basin; CIOB: Central Indian Ocean Basin; CIR: Central Indian Ridge; CKP: Central Kerguelen Plateau; CLR: Chagos Laccadive Ridge; CR: Carlsberg Ridge; KFZ: Kerguelen FZ; MAB: Mascarene Basin; MB: Madagascar Basin; MP: Madagascar Plateau; NER: Ninetyeast Ridge; NKP: Northern Kerguelen Plateau; SEIR: Southeast Indian Ridge; SKP: Southern Kerguelen Plateau; SL: Sri Lanka; ST: Sunda Trench; SWIR: Southwest Indian Ridge; WB: Wharton Basin.

Fig. 2: (a) Satellite gravity map of the northeastern Indian Ocean (version 23.1; Sandwell et al., 2014). Published magnetic isochrons are shown as blue lines and some are identified (Talwani et al., 2016, Desa and Ramana, 2016; Desa et al., 2009; 2018; 2019). Middle Cretaceous geomagnetic field incursions Q1, M-3r and Q2 represent 92, 102 and 108 Ma respectively (Granot et al., 2012; Desa and Ramana, 2016). Fracture zones are marked as dashed black lines (Wessel et al., 2015). Our track SK101 is shown as thick line in red. The extent of deformation is shown in dashed orange outline (Gordon et al., 1998). Drill sites are marked as black circles. The gravity low of the 85°E Ridge is marked as dashed pink outline. Large igneous provinces are marked as thin red outlines (Eldholm and Coffin, 2000). The study area is shown in a red box. 86E FZ: 86°E Fracture Zone; ANS: Afanasy Nikitin Seamount chain; CIOB: Central Indian Ocean Basin; CR: Comorin Ridge; NER: Ninetyeast Ridge; ST: Sunda Trench.

(b) Predicted bathymetry of the study area in greyscale (version 18.1; Smith and Sandwell, 1997). Drill sites are shown as black circles and numbered. Our track SK101 is shown as a thick line in different colors according to its seismic records (A to E) which are shown in figures 3-7. Published tracks used in the present study are marked in different colours as per legend. Their source details are as follows: 1: GeoB97-020/027 (Schwenk and Speiss, 2009); 2: antipode11 (Curry and Munasinghe, 1989); 3: Levchenko (1992); 4: Delescluse et al. (2008); 5: AWI-20170400 (Altenbernd et al., 2020); 6: Neprochnov et al. (1988); 7: AS10-01 & 02 (Krishna et al., 1998). Fracture zones are marked as dashed black lines (Wessel et al., 2015). The extent of deformation is shown in dashed orange outline (Gordon et al., 1998). Earthquake epicentres (USGS, 2020) are marked as red stars. The sonobuoy station 264 is shown as yellow star (Naini and Leyden, 1973). The gravity low of the 85°E Ridge (85ER) is marked as dashed pink outline. The outline of the arcuate gravity low is marked as dashed green outline. Locations of seismic records depicted in figure 9 are marked as blue boxes. 86E FZ: 86°E Fracture Zone.

Fig. 3: Un-interpreted (a) and interpreted (b) seismic section A (shot: 65-7464) of the transect SK101. Five seismic horizons H1 to H5 which divide the sediment load into 6 sequences sed1 to sed6 are marked in different colours. The acoustic basement is marked in brown. Drill sites and crossings of published profiles are indicated. Red line indicates a fault. Yellow diamond denotes location of an earthquake epicentre. Basement highs and deformational highs are identified. Deformation signatures are seen in sediment and basement. Flower structures are observed occasionally. Boxes denote the extent of seismic record enlarged in figure 9.

Fig. 4: Un-interpreted (a) and interpreted (b) seismic section B (shot: 1-5857) of the transect SK101, Remaining information as in Figure 3.

Fig. 5: Un-interpreted (a) and interpreted (b) seismic section C (shot: 400-5113) of the transect SK101. Remaining information as in Figure 3.

Fig. 6: Un-interpreted (a) and interpreted (b) seismic section D (shot: 5116-10000) of the transect SK101. Remaining information as in Figure 3.

Fig. 7: Un-interpreted (a) and interpreted (b) seismic section E (shot: 1-5274) of the transect SK101. Remaining information as in Figure 3.

Fig. 8: Composite figure depicting various parameters along the transect SK101.

(a) magnetic (black), gravity (red) and bathymetry (blue) signatures. The numbers in italics represent the shot points on the seismic record. Basement highs and deformational highs are identified.

(b) Line drawing depicting the horizons H1 to H5 in different colours, seafloor and basement in sec TWT along the transect. The locations of published drill sites and seismic profiles are indicated. The extent of the seismic records A to E is depicted by a black line with arrows. Red arrow depicts the location of the step in the basement coinciding with the abrupt change in magnetic pattern.

(c) Line drawing of the computed sediment thickness (blue) and sediment corrected basement depth (black) in km. Estimated crustal ages in Ma are plotted as red squares. Ages for basement highs are suspect and hence not included.

Fig. 9: Enlarged seismic records depicting key characteristics in the sediment load and basement. Red line indicates a fault. The five seismic horizons H1 to H5 are marked in different colours. Their locations are given in figure 2b. ACB: Acoustic Basement

- (a) Figure depicting the folding of the lower sediment sequences and basement over the 86°E FZ. Flower structures depicting small-scale compression are observed in this area.
- (b) A fully buried basement high appears to have formed by piercing the original horizontal basement forming a volcanic knoll. Termination of the lower sediments at its flanks implies that this high existed before their deposition.
- (c) Figure depicting part of the deformational high T1 located over a NW-SE trending fracture zone. The seabed is uneven and the upper strata is heavily faulted. A prominent basement undulation (~0.4 sec TWT) is seen between two flower structures.
- (d) Figure depicting a prominent step in the basement (~0.4 sec TWT) while the horizon H1 is nearly flat. This probably suggests the concurrent presence of oceanic crust of different ages at this location.

Fig. 10: Plate reconstruction model depicting the oceanic crust generated between India and Antarctica by 80 Ma (Matthews et al., 2016). India is in its present day position. Relevant fracture zones are shown as dashed black lines. 85°E Ridge gravity low is marked in magenta. Major isochrons are marked as thin black continuous lines, some are highlighted in different colors and labelled. The 80 Ma plate boundaries are outlined in green. Our transect is shown in different colors as per seismic records. The red rectangle on the 100 Ma isochron marks the location of the 0.4 sec TWT step in the basement (Fig. 9d). A change in spreading direction is obvious between 108 and 100 Ma. Conjugate corridor (dashed blue outlines) illustrates excess crust on Antarctica plate as compared to Indian plate, between 100 and 83 Ma. Rotation pole parameters: latitude: 12.96; longitude: 7.21; angle: 59.03. CR: Conrad Rise; EB: Elan Bank; M: Madagascar; SKP: Southern Kerguelen Plateau; SL: Sri Lanka.



### List of Tables:

Table 1: Major reflectors from published seismic/drill results and the corresponding horizons inferred in this study.

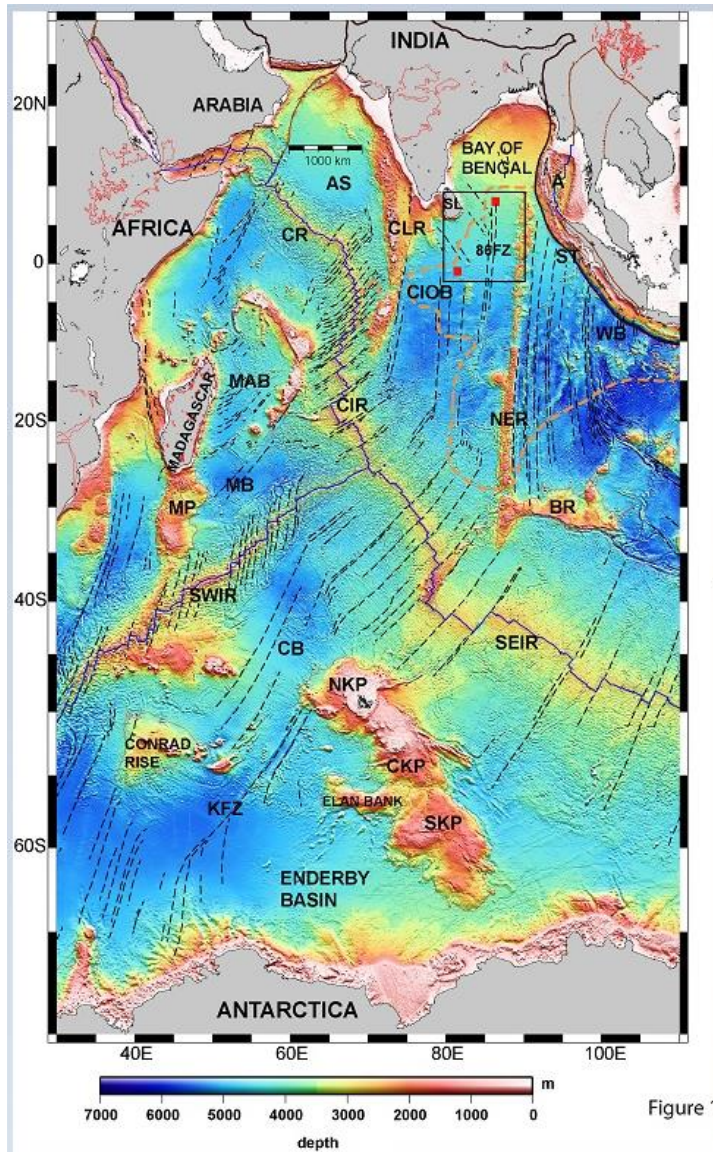
Table 2: Summary of the sequences inferred along the transect SK101. The transect is divided into three parts based on the locations of the published seismic velocities.

Table 1: Major reflectors from published seismic/drill results and the corresponding horizons inferred in this study.

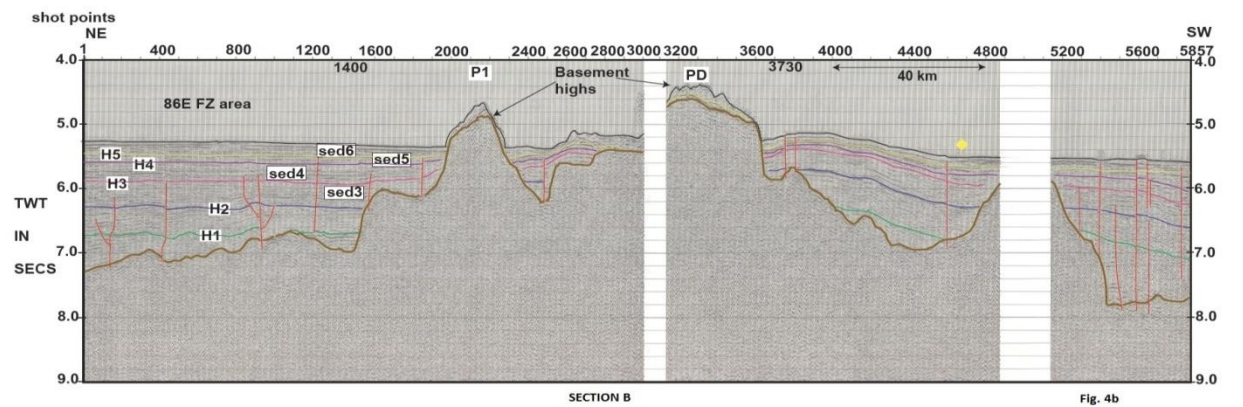
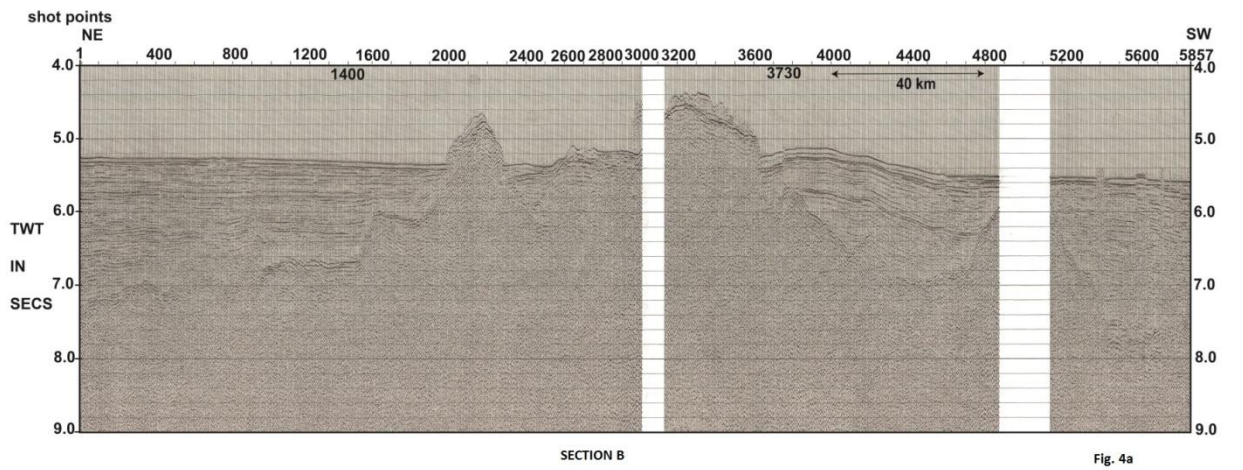
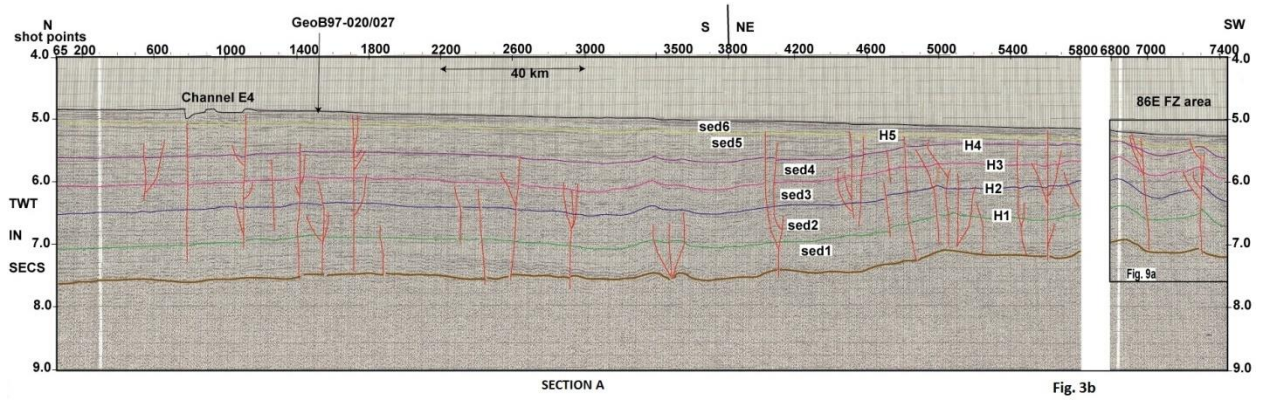
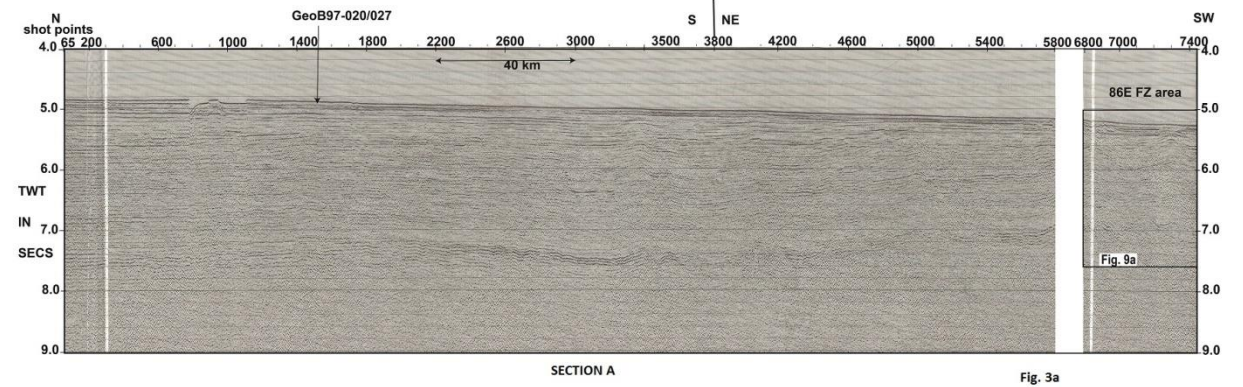
DSDP218/IODP1455/ GeoB97-020/027			ODP718/ AS10-01			AWI-20170400		This study
reflector	sec TWT	meters	reflector	sec TWT	meters	reflector	sec TWT	Horizon
Pleistocene Unconformity	5.1	78	B	6.4	104	R2	6.05	H5
Pliocene Unconformity	5.33	~250	AA	6.47	135	-	-	H4
Miocene Unconformity	5.53	400	A	6.55	275	R1	6.55	H3
12 ma	6.08	940	12ma	6.95	660	Top of sed3	7.2	H2
Eocene Unconformity	-	-	-	-	-	Top of sed4	7.9	H1

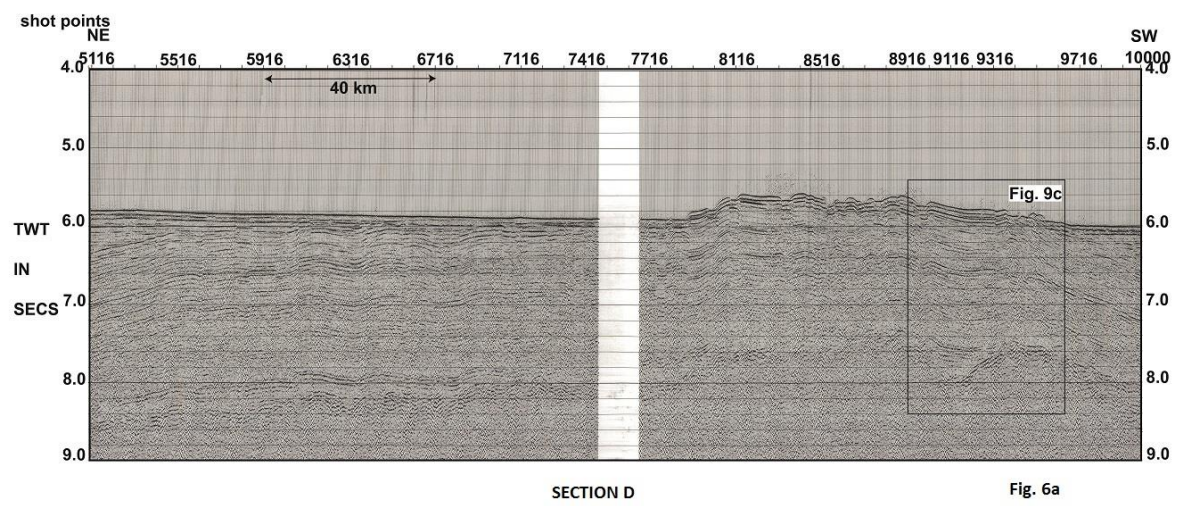
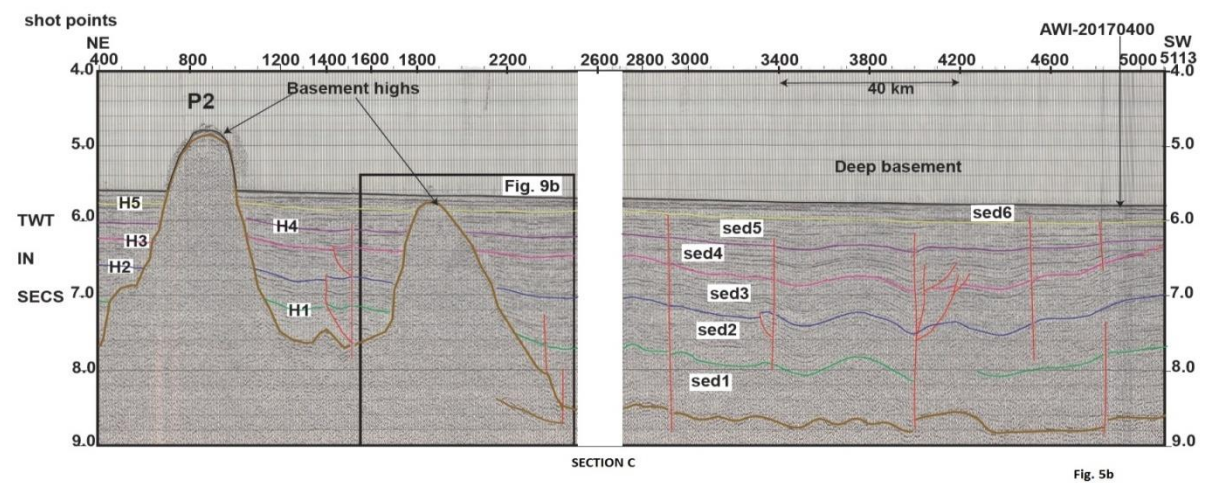
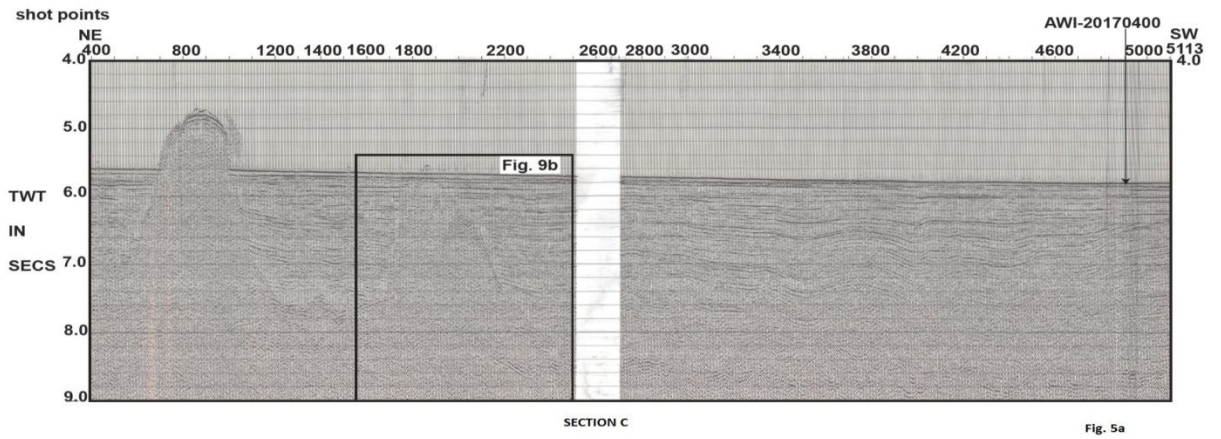
Table 2: Summary of the sequences inferred along the transect SK101. The transect is divided into three parts based on the locations of the published seismic velocities.

Seq- uence	Horizon above the se- quence	Along sections A and B (till shot 1480)		Along sections C (beyond shot 2200) and D		Along section E (beyond shot 471)	
		<i>Velocity (km/s) (Naini and Leyden 1973)</i>	<i>Average thickness in km</i>	<i>Velocity (km/s) (Altenbernd et al., 2020)</i>	<i>Average thickness in km</i>	<i>Velocity (km/s) (Bull and Scrutton, 1990b)</i>	<i>Average thickness in km</i>
Sed6	seabed	2.0	0.18	2.0	0.14	2.0	0.09
Sed5	H5	2.2	0.32	2.0	0.13	2.0	0.13
Sed4	H4	2.4	0.44	2.1	0.14	2.0	0.18
Sed3	H3	3.0	0.58	2.5	0.59	2.5	0.58
Sed2	H2	3.8	0.91	3.1	1.13	3.3	1.11
Sed1	H1	4.6	1.12	4.1	1.55	4.1	0.67









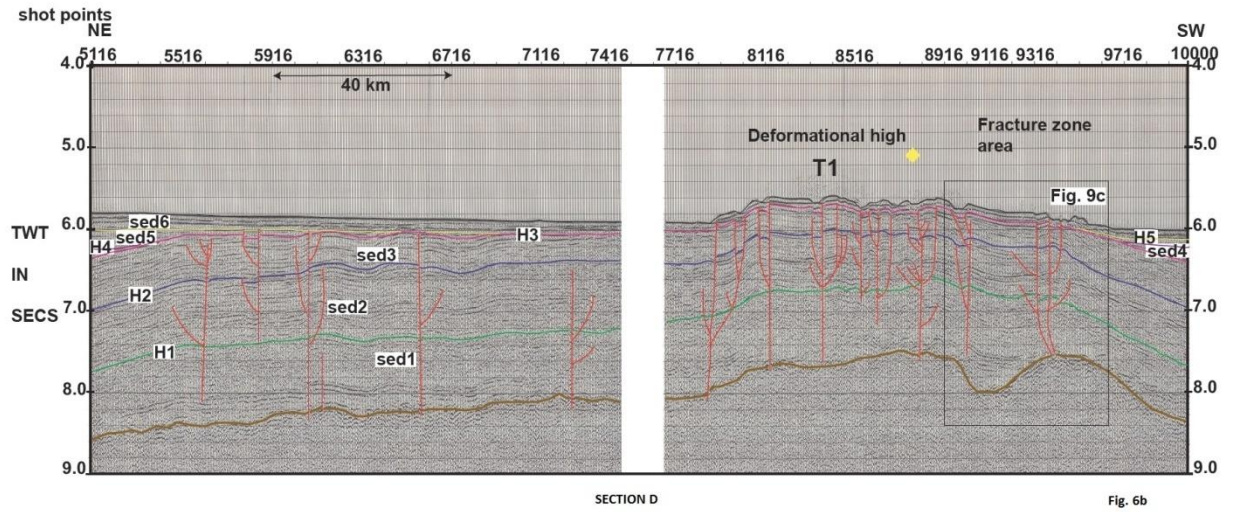


Fig. 6b

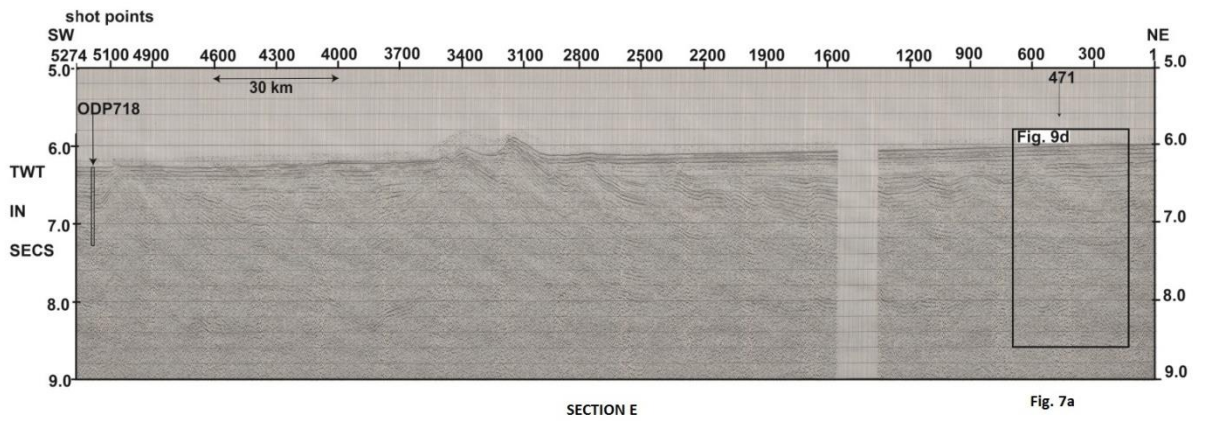


Fig. 7a

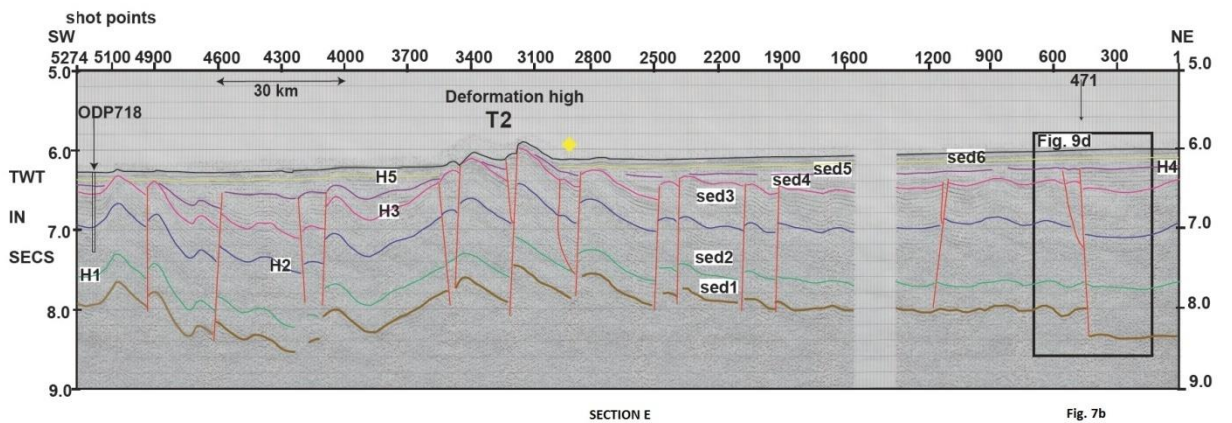


Fig. 7b

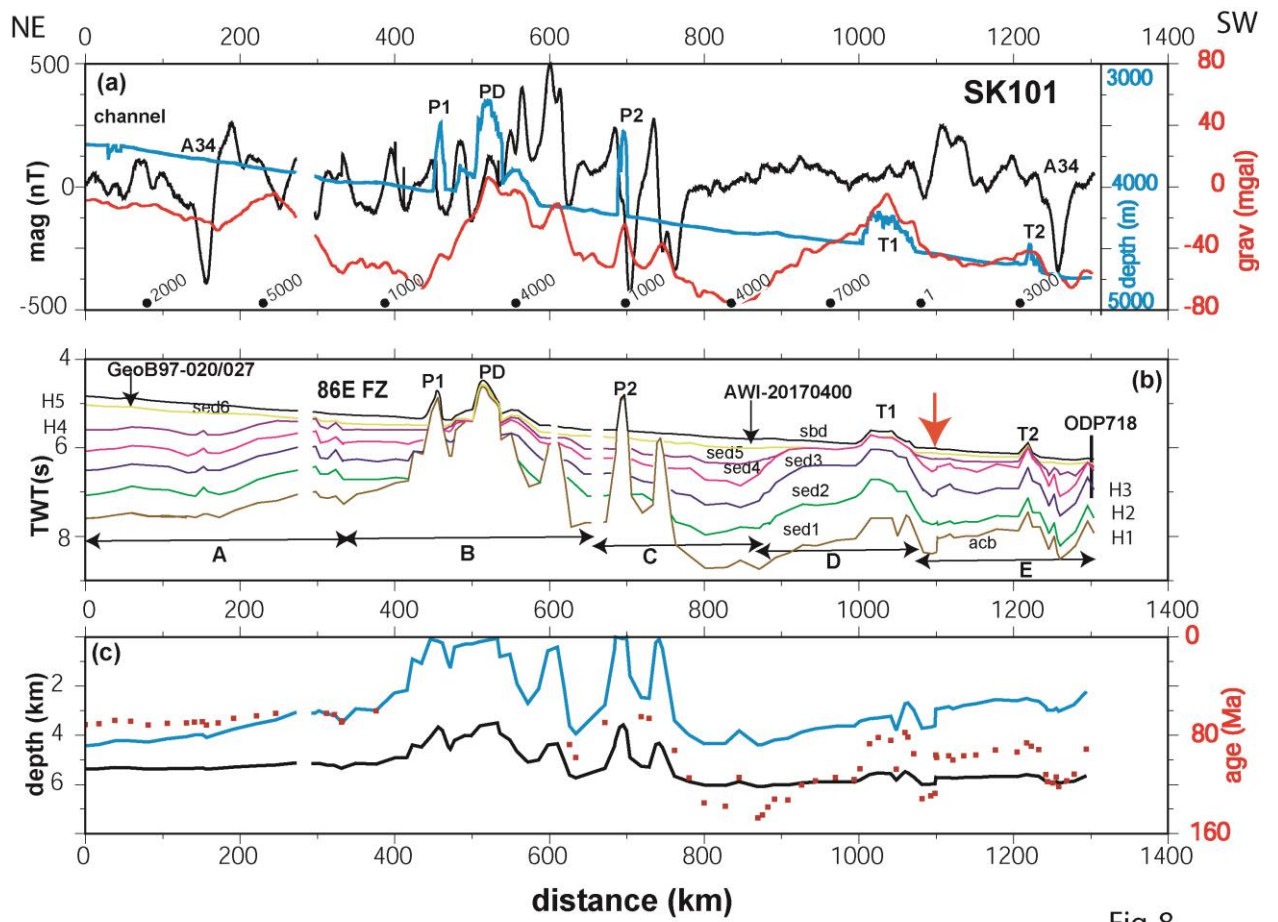


Fig.8

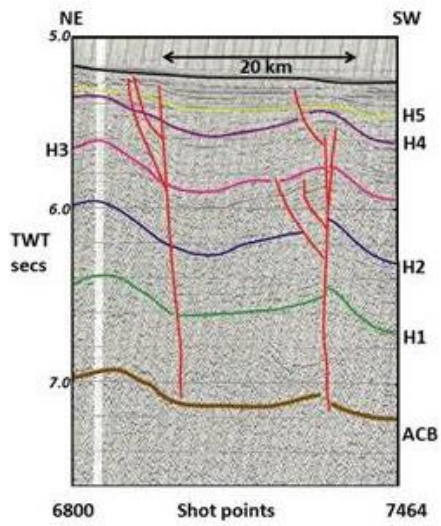


Fig. 9a

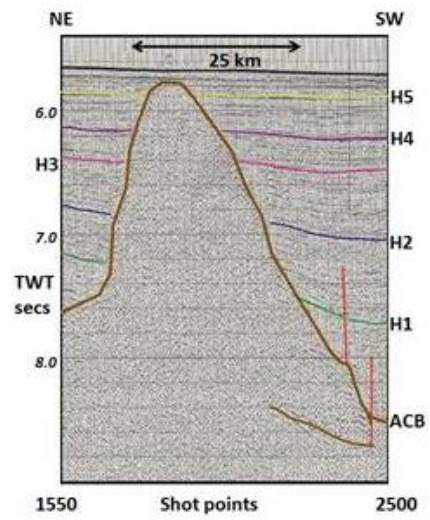


Fig. 9b

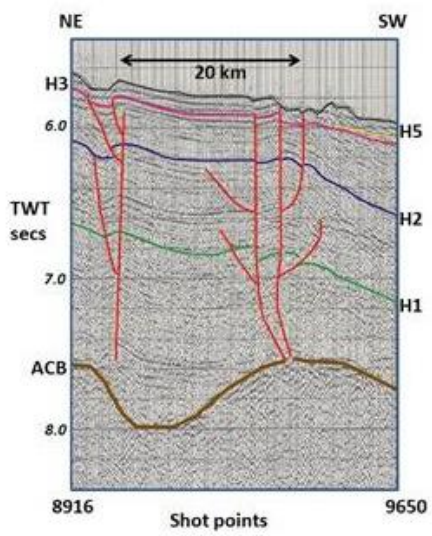


Fig. 9c

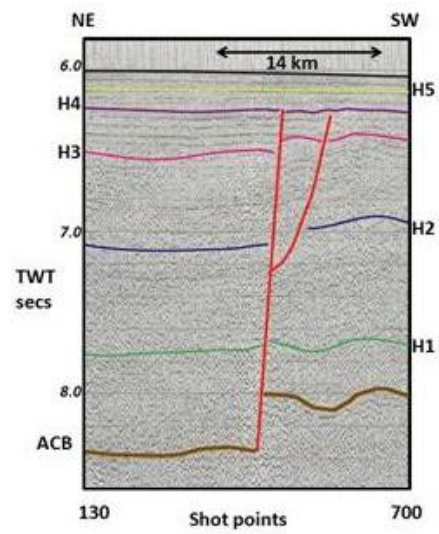


Fig. 9d



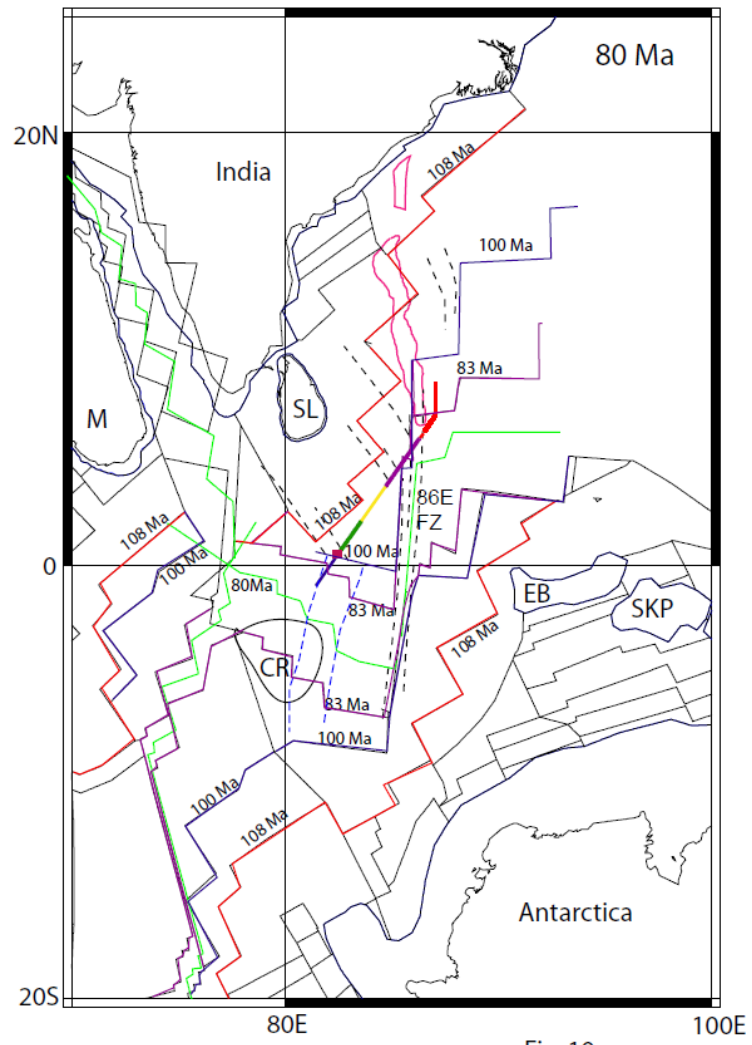


Fig. 10